



Title	Structure of Atg5-Atg16, a complex essential for autophagy.
Author(s)	Matsushita, Minako; Suzuki, Nobuo N.; Obara, Keisuke et al.
Citation	Journal of Biological Chemistry, 282(9), 6763-6772 https://doi.org/10.1074/jbc.M609876200
Issue Date	2007-03-02
Doc URL	https://hdl.handle.net/2115/22079
Rights	Copyright © 2007 by the American Society for Biochemistry and Molecular Biology
Type	journal article
File Information	JBC282-9.pdf



STRUCTURE OF ATG5·ATG16, A COMPLEX ESSENTIAL FOR AUTOPHAGY*

Minako Matsushita¹, Nobuo N. Suzuki¹, Keisuke Obara², Yuko Fujioka¹, Yoshinori Ohsumi² and Fuyuhiko Inagaki¹

From ¹Department of Structural Biology, Graduate School of Pharmaceutical Sciences, Hokkaido University, N-21, W-11, Kita-ku, Sapporo 001-0021, Japan, ²Division of Molecular Cell Biology, National Institute for Basic Biology, Myodaiji, Okazaki 444-8585, Japan.

Running title: Structure of Atg5·Atg16 complex

Address correspondence to: Fuyuhiko Inagaki, Department of Structural Biology, Graduate School of Pharmaceutical Sciences, Hokkaido University, N-21, W-11, Kita-ku, Sapporo 001-0021, Japan, Tel. +81-11-706-9011; Fax. +81-11-706-9012; E-Mail: finagaki@pharm.hokudai.ac.jp

Atg5 is covalently modified with a ubiquitin-like modifier, Atg12, and the Atg12-Atg5 conjugate further forms a complex with the multimeric protein Atg16. The Atg12-Atg5·Atg16 multimeric complex plays an essential role in autophagy, the bulk degradation system conserved in all eukaryotes. We report here the crystal structure of Atg5 complexed with the N-terminal region of Atg16 at 1.97 Å resolution. Atg5 is comprised of two ubiquitin-like domains that flank a helix-rich domain. The N-terminal region of Atg16 has a helical structure and is bound to the groove formed by these three domains. *In vitro* analysis showed that Arg-35 and Phe-46 of Atg16 are crucial for the interaction. Atg16 with a mutation at these residues failed to localize to the pre-autophagosomal structure, and could not restore autophagy in Atg16 deficient yeast strains. Furthermore, these Atg16 mutants could not restore a severe reduction in the formation of the Atg8-phosphatidylethanolamine conjugate, another essential factor for autophagy, in Atg16 deficient strains under starvation conditions. These results taken together suggest that the direct interaction between Atg5 and Atg16 is crucial to the performance of their roles in autophagy.

Autophagy mediates the bulk degradation of cytoplasmic components in lysosomes/vacuoles (1,2) and plays a critical role in numerous biological processes, such as neurodegeneration and pathogen infection as well as in the survival response during neonatal starvation (3-7). In autophagy, a double-membrane structure called an autophagosome sequesters a portion of cytoplasm and fuses with the lysosome/vacuole to deliver its contents into the organelle lumen.

Atg5 was identified together with other Atg proteins by genetic screening in the yeast *Saccharomyces cerevisiae* (8). Since Atg5 has little sequence homology with proteins with known functions, it is difficult to predict its structure and function from the sequence. Thus far, biochemical analyses have shown that Lys-149 of Atg5 is conjugated to Atg12, a ubiquitin-like modifier, dependent on ATP and two enzymes, Atg7 (E1-like) and Atg10 (E2-like) (9,10). Compared with other ubiquitin-like modifications, the Atg12-modification is unique in that it is irreversible and constitutive. The majority of Atg5 and Atg12 exist as Atg12-Atg5 conjugates irrespective of whether autophagy is induced or not, and behave as a single protein (11). In yeast, the Atg12-Atg5 conjugate localizes to the pre-autophagosomal structure (PAS), a putative center for autophagosome formation (12). All Atg proteins involved in Atg12-Atg5 conjugation are also conserved in mammals. Localization studies of the Atg12-Atg5 conjugate in ES cells using GFP-fused Atg5 showed that the Atg12-Atg5 conjugate is translocated from the cytosol to the isolation membranes upon nutrient deprivation and, immediately upon completion of autophagosome formation, the Atg12-Atg5 conjugate dissociates from the membrane, suggesting that it plays a significant role in autophagosome formation (13).

In addition to the covalent interaction with Atg12, Atg5 interacts non-covalently with a multimeric protein, Atg16 (14). Atg16 was originally obtained from a two-hybrid screen using Atg12 as a bait, and was later confirmed to interact with Atg5 but not Atg12 *via* its N-terminal region. Since Atg16 self-assembles *via* its carboxy-terminal coiled-coil motif (residues 58-123), the Atg12-Atg5 conjugate forms a multimeric complex with Atg16 (11,14).

Further, as the majority of Atg12-Atg5 conjugates form a complex with Atg16 constitutively, the conjugates should function as a complex with Atg16 during autophagosome formation. In fact the Atg12-Atg5 conjugate cannot localize to the PAS in $\Delta atg16$ yeast strains (12,15). In mammals, Atg16L, a functional counterpart of yeast Atg16, was shown to localize to the isolation membranes together with the Atg12-Atg5 conjugate during autophagosome formation (16).

Although the significance of the Atg12-Atg5-Atg16 complex in autophagosome formation has been shown, its molecular function is still not clearly understood. One identified function of the Atg12-Atg5 conjugate is to promote the formation of the Atg8-phosphatidylethanolamine (PE) conjugate, the other conjugate essential for autophagosome formation, and the targeting of the Atg8-PE conjugate to the PAS (12). Atg8 is a ubiquitin-like modifier that is first processed by a cysteine protease, Atg4 (17). The processed Atg8 is conjugated to PE dependent on ATP and two enzymes, Atg7 (E1-like) and Atg3 (E2-like) (18). Although Atg3, Atg7, Atg8 (processed form), and ATP are sufficient for Atg8-PE conjugation *in vitro* (19), the Atg12-Atg5 conjugate is also required for Atg8-PE conjugation *in vivo* (12). The expression of Atg8 is dramatically enhanced upon nutrient depletion. Under such conditions, Atg16 is also required for the efficient formation of Atg8-PE (12). However, the molecular mechanism by which the Atg12-Atg5 conjugate and Atg16 promote Atg8-PE formation is not clear. Recently, we reported the crystal structure of plant Atg12 and revealed that Atg12 is a ubiquitin-fold protein (20). However, structural information on Atg5 and Atg16 has been thoroughly lacking, preventing us from elucidating the molecular functions of the Atg12-Atg5-Atg16 complex. In this report, we describe the first structure of Atg5 in complex with the N-terminal region of Atg16. Furthermore, based on structural information, Atg16 mutants that lost the binding affinity to Atg5 were constructed and used to clarify the significance of the direct interaction between Atg5 and Atg16 in autophagy.

EXPERIMENTAL PROCEDURE

Protein expression and purification - Expression and purification of Atg5-Atg16(1-46) and Atg5-Atg16(1-57) as well as the construction of

the expression vector of hexa-histidine-tagged Atg5 were described previously (21). The expression vectors of GST-fused Atg16 and its mutants were constructed as follows. The full-length ATG16 gene was amplified by polymerase chain reaction (PCR) and inserted into pGEX-6P-1 (GE Healthcare Bio-Sciences). Mutations leading to the indicated amino acid substitutions were introduced by PCR-mediated site-directed mutagenesis. All the constructs were sequenced to confirm their identities, and were expressed in *Escherichia coli* strain BL21 (DE3) cells. After cell lysis, GST-fused Atg16 and its mutants were purified by sequential chromatography using a glutathione-Sepharose 4B column (GE Healthcare Bio-Sciences) and a Superdex200 gel filtration column (GE Healthcare Bio-Sciences). Hexa-histidine-tagged Atg5 was purified by sequential chromatography using a Ni-NTA column (QIAGEN) and a Superdex75 gel filtration column (GE Healthcare Bio-Sciences).

Diffraction data collection - Crystallization of Atg5-Atg16(1-46) and Atg5-Atg16(1-57) was performed and four crystal forms (I-IV) were obtained as described previously (21). Crystal form I (Atg5-Atg16(1-46) complex) was used for phase determination, and crystal form IV was used for structure determination of Atg5-Atg16(1-57). Collection of native data for Atg5-Atg16(1-46) and Atg5-Atg16(1-57) for final refinement was described previously (21). Native data for phase determination as well as the mercury and platinum derivative data for Atg5-Atg16(1-46) were collected on Rigaku R-AXIS IV and VII imaging plate detectors using Cu $K\alpha$ radiation from an in-house Rigaku rotating-anode X-ray generator. MAD data for the SeMet-substituted crystal of Atg5-Atg16(1-46) at three wavelengths were collected on the ADSC Quantum 315 CCD detector at the BL41XU beamline, SPring-8. All diffraction data were indexed, integrated and scaled with HKL2000 (22).

Structure determination - The initial phasing was performed by the combination of MIR and MAD methods against Atg5-Atg16(1-46) crystals using the CNS program suite (23). After MIR phases were calculated using the data between 50 and 3.5 Å resolution for mercury and platinum derivatives, 35 selenium sites for SeMet-substituted crystals were identified from the anomalous difference Fourier map calculated using the peak data and the MIR phases. MAD phases were then calculated using the data

between 50 and 3.0 Å resolution for a SeMet-substituted crystal at three wavelengths, and were combined with the MIR phases. After density modification, the obtained phases were used to calculate the electron density map for model building. Model building was performed manually using programs O (24) and COOT (25), and crystallographic refinement was performed using CNS. The structure of Atg5·Atg16(1-57) was determined by the molecular replacement method using the structure of Atg5·Atg16(1-46) as a search model.

In vitro pull-down assay - GST-fused Atg16 and its mutants were mixed with hexa-histidine-tagged Atg5 in phosphate-buffered saline and incubated at 277 K for 30 min. Subsequently, a slurry of glutathione-Sepharose 4B was added, followed by further incubation at 277 K for 30 min. After washing three times with phosphate-buffered saline, proteins were incubated with 10 mM glutathione in 50 mM Tris-HCl buffer at pH 8.0. The elutes were subjected to 15% SDS-PAGE and stained with Coomassie Brilliant Blue.

In vivo assay – The significance of the complex formation between Atg16 and Atg5 *in vivo* was examined as follows. Point mutations were introduced by PCR-based site-directed mutagenesis using pRS314- or pRS424-based plasmids containing the *ATG16-HA* gene (14) as templates. Successful introduction of the point mutations was confirmed by sequencing. These plasmids were introduced into *Δatg16::LEU2* cells on a SEY6210 (*MATα leu2 ura3 his3 trp1 lys2 suc2*) (26) or BJ2168 (*MATα leu2 trp1 ura3 pep4-3 prb1-1122 prc1-407*; Yeast Genetic Stock Center) background. SEY6210 *Δatg16::LEU2* cells expressing Atg16 mutants were cultured in SD + casamino acids (CA) +AdeUra medium to logarithmic phase and then transferred to SD (-N) medium. After culture for 4 h in SD (-N) medium, cells were collected. The lysates were prepared by the alkaline-TCA method, resuspended in SDS-PAGE sample buffer, and separated by SDS-PAGE, with subsequent immunoblotting using anti-API and anti-Atg8 antibodies. Signals were detected using an ECL system (GE Healthcare, Buckinghamshire, UK) with a bioimaging analyzer (LAS1000; Fujifilm, Tokyo, Japan). To separate lipidated and non-lipidated Atg8 by mobility, separating gel containing 6 M urea was used (17). Accumulation of autophagic bodies was examined using BJ2168 *Δatg16::LEU2* cells expressing the Atg16 mutants. Cells in

logarithmic phase of growth were transferred to S (-NC) medium. After culture for 4 h in S (-NC) medium, cells were observed by phase-contrast microscopy. YFP-tagged Atg16 mutants were engineered by PCR-based site-directed mutagenesis using a plasmid containing the *ATG16-YFP* gene (12) as a template. Successful introduction of the point mutations was confirmed by sequencing. The plasmids were introduced into SEY6210 *Δatg16::LEU2* cells. Cells with the plasmids were cultured in SD + CA +AdeUra medium to logarithmic phase and transferred to SD (-N) medium. After culture for 4 h in SD (-N) medium, cells were observed under an inverted fluorescence microscope (IX-81; Olympus, Tokyo, Japan) equipped with a cooled CCD camera (CoolSNAP HQ; Nippon Roper, Tokyo, Japan). Images were acquired using MetaMorph software (Universal Imaging, Buckinghamshire, UK) and processed using Adobe PhotoShop software (Adobe Systems, Mountain View, CA.).

RESULTS

Overall structure of the Atg5·Atg16(1-57) complex - As the N-terminal half (residues 1-87) of Atg16 was reported to be sufficient for complex formation with Atg5 (14), we constructed two lengths of Atg16, Atg16(1-46) and Atg16(1-57). Both were found to form a stable complex with Atg5 (data not shown). We prepared and crystallized both Atg5·Atg16(1-46) and Atg5·Atg16(1-57) complexes (21), and determined their structures. The structures of the two complexes were essentially identical except for residues 47-57 of Atg16; therefore, we refer only to the structure of the Atg5·Atg16(1-57) complex hereafter. The structure of Atg5·Atg16(1-57) was refined against 1.97 Å data to an *R*-factor of 0.215 and a free *R*-factor of 0.245. The regions corresponding to amino acids 1-310 of Atg5 and 22-57 of Atg16 were modeled along with 244 water molecules (Fig. 1A). Residues 65-68, 100-108, and 243-246 of Atg5 and residues 1-21 of Atg16 lacked defined electron density and were omitted from the model. The Atg5·Atg16(1-57) complex has an α/β fold comprised of ten β -strands (β 1- β 10) and ten α -helices (α 1- α 9 of Atg5 and a helix of Atg16), with overall approximate dimensions of 65 x 45 x 45 Å.

Atg5 is comprised of three domains – Fig. 1B shows the topology of Atg5. Atg5 is comprised

of two ubiquitin-like domains that flank a helix-rich domain. We named the N- and C-terminal ubiquitin-like domains UblA (yellow) and UblB (red), respectively, and the helix-rich domain between UblA and UblB, HR (green). The linker regions connecting HR with UblA and UblB were named L1 and L2, respectively. In addition to the three domains and two linkers, Atg5 has an additional α -helix (α 1) at its N-terminus (orange). A color-coded ribbon diagram of Atg5 domains is shown in Fig. 1C.

Both UblA and UblB are comprised of a five-stranded β -sheet and two α -helices, which is a conserved feature in all ubiquitin superfamily proteins. Comparison of UblA and UblB of Atg5 with the PDB database using the Dali search engine revealed that both domains show structural similarity to ubiquitin (PDB code 1UBI) and ubiquitin-like proteins, including LC3 (PDB code 1UGM; a mammalian ortholog of yeast Atg8) and AtATG12b (PDB code 1WZ3; a plant ortholog of yeast Atg12) with a Z-score of 5.8-8.2 and an rmsd of 2.3-3.0 Å for 66-80 residues. Fig. 2 shows the sequence alignment of Atg5 homologs, in which Val, Leu, Ile, Pro, Met, Phe, Tyr, and Trp are all considered to be hydrophobic residues and colored yellow, and other conserved residues are colored cyan. The sequences of ubiquitin and LC3 are also aligned based on their three-dimensional structures. Although the sequence identities of UblA and UblB with ubiquitin and LC3 are low (11-16%), hydrophobic residues that constitute the ubiquitin core are conserved, indicating that the two ubiquitin-like domains are part of the conserved architecture in Atg5 family proteins.

HR is comprised of three long and one short α -helices that form a helix-bundle structure. Comparison of HR with the PDB database using the Dali search engine showed that HR is structurally similar to the domain III of CysG, a multifunctional siroheme synthase (27) (PDB code 1L3I), with a Z-score of 4.8 and an rmsd value of 2.9 Å for 53 residues. HR also shows weak structural similarity to CUE (coupling of ubiquitin conjugation to ER), a ubiquitin binding domain, with a Z-score of 2.2 and an rmsd value of 3.4 Å for 40 residues. Eleven hydrophobic residues constituting the core of HR are conserved among Atg5 homologs (Fig. 2), indicating that HR is also part of the conserved architecture in Atg5 family proteins. Lys-149, the conjugation site for Atg12, is

located on α 4 of HR and exposes its side-chain (Fig. 1).

Structural basis of the Atg5 architecture - Although each domain constituting Atg5 has a common fold, the overall architecture of Atg5 is unique and no similar structures have been reported. Three domains, two linkers, and α 1 form many interactions with each other, and are packed into a globular structure. Amongst all pairs, the UblA - UblB pair forms the largest interaction surface (1,574 Å²). α 3 of UblA is located on the central β -sheet of UblB, and is surrounded by three loops connecting β 6- β 7, β 8- β 9, and α 9- β 10 of UblB (Fig. 3A, left), thus forming a wide point of contact with UblB. This binding mode is partly similar to that between ubiquitin and the ubiquitin-interacting motif (UIM) (28), although the direction of the bound helix is inverse (Fig. 3A, right).

Compared with the interaction surface between UblA and UblB, those between UblA and HR (657 Å²) and between UblB and HR (824 Å²) are rather small. However, UblB and HR form extensive hydrophobic interactions with each other (Fig. 3B, left). Pro-201 and Phe-276 of UblB interact with Val-151 and Ile-154 of HR, whereas Phe-273 of UblB interacts with Trp-144 and Val-177 of HR. Phe-273 also interacts with Tyr-44 and Pro-86 of UblA, thus playing a crucial role in gathering the three domains. Interestingly, the loop connecting α 9 and α 10 of UblB, which plays a major role in these interactions, is both sequentially and structurally similar to the equivalent loop of LC3 (Fig. 2, 3B right). In LC3, the loop is involved in the interaction with two N-terminal α -helices, α 1 and α 2 (29). Val-151 and Ile-254 of HR and Pro-201 and Ile-203 of UblB are also conserved in LC3, and are involved in the interaction between the ubiquitin-fold region and α 2 of LC3. Thus, the ubiquitin folds in both Atg5 and LC3 utilize the common residues for the construction of the architecture of each protein.

Sequence alignment shows that in addition to the three domains, α 1 and L1 are also conserved among Atg5 homologs, whereas L2 is not conserved at all (Fig. 2). L1 has four hydrophobic residues, Leu-126, Pro-127, Ile-131, and Pro-132, which are conserved among Atg5 homologs (Fig. 2). Leu-126 and Pro-132 interact with each other, whereas Pro-127 and Ile-131 interact with the conserved tryptophans, Trp-73 and Trp-83, of UblA, respectively (Fig. 3C). Through these interactions, L1 takes on a rigid

conformation and may contribute to fixing the UblA–HR arrangement. In addition to the interactions described above, the interactions mediated by $\alpha 1$ seem to play critical roles in the formation of the Atg5 architecture. $\alpha 1$ has two conserved hydrophobic residues, Leu-8 and Trp-9 (Fig. 2); Trp-9 interacts with conserved hydrophobic residues, Val-177, Phe-182, and Phe-185, of HR, whereas Leu-8 interacts with a conserved hydrophobic residue, Leu-270, of UblB (Fig. 3D). Ile-4 of $\alpha 1$, which is partially conserved, also interacts with Leu-270. Thus $\alpha 1$, which is located prior to the N-terminus of UblA, plays an essential role in the assembling of the three domains. In addition to the intramolecular interactions, Ile-4 and Leu-8 of $\alpha 1$ also interact with the hydrophobic residues in Atg16 (Fig. 3D).

Structural basis of the interaction between Atg5 and Atg16 - Atg16(1-57) is comprised of an α -helix (residues 22-40) and its downstream loop (residues 41-57). The helix moiety of Atg16 is bound to the groove formed by UblA, UblB, and $\alpha 1$, whereas the loop moiety is mainly bound to UblA (Fig. 4A). The N-terminal residues (residues 1-21) of Atg16 were disordered in the crystal, and may not interact with Atg5.

The detailed interactions observed between Atg5 and Atg16 are shown in Fig. 4B. The side-chains of Asp-25, Arg-31, Arg-35, Asn-36, Glu-39, Asp-48, and Asn-49 of Atg16 form hydrophilic interactions with Atg5. In particular, the side-chains of Arg-35, Asn-36, and Glu-39 are clustered at the deep groove at the boundary of UblA, UblB, and $\alpha 1$ of Atg5, and form extensive hydrophilic interactions with these three regions. Three glycine residues (Gly-11, Gly-88, and Gly-254), together with Arg-41 and Asp-92 of Atg5, which constitute the deep groove, are well conserved among Atg5 homologs (Fig. 2). In addition to the hydrophilic interactions, Atg16 also forms hydrophobic interactions with Atg5. Ile-255, Ile-257, Pro-258, Met-261, and Leu-270 of UblB and Ile-4, Leu-7, and Leu-8 of $\alpha 1$ form an extensive hydrophobic surface on which Met-24, Leu-27, Leu-28, Ile-29, and Leu-32 of Atg16 are bound. Furthermore, Leu-16, Arg-36, Leu-113, and Phe-115 of UblA form a hydrophobic cavity in which Phe-46 of Atg16 is bound. In contrast, residues 50-57 of Atg16 have few interactions with Atg5, which is consistent with the observation that Atg16(1-46) is sufficient for

complex formation with Atg5.

To identify the residues of Atg16 crucial for the interaction with Atg5, an *in vitro* pull-down assay was performed using hexa-histidine-tagged Atg5 and GST-fused Atg16 mutants. Eleven Atg16 residues (labeled in Fig. 4A) were mutated with alanine. As shown in Fig. 4C, Arg-35 and Phe-46, especially Arg-35, were crucial for the interaction between Atg5 and Atg16.

Significance of the Atg5 - Atg16 interaction for both Atg8 lipidation and autophagy - To reveal the significance of the direct interaction between Atg5 and Atg16, we measured the *in vivo* activities of two Atg16 mutants, R35A and F46A, that lack binding affinity to Atg5 *in vitro*. As a control, the Atg16 D25A mutant, which retains binding affinity to Atg5 *in vitro*, was also assayed. The activity of Atg16 mutants was first assayed by monitoring the maturation of proform of API (aminopeptidase I), which is transported into vacuoles *via* the cytoplasm-to-vacuole targeting (Cvt) pathway or by autophagy under nutrition-rich and starvation conditions, respectively. The protein is then processed into a mature form within vacuoles. API maturation, which was not observed in $\Delta atg16$ cells, was restored in cells expressing the Atg16 D25A mutant to a similar extent to those expressing wild-type Atg16 (Fig. 5A). In contrast, there was little restoration of API maturation in cells expressing the R35A or F46A mutants of Atg16 (Fig. 5A). Next, the accumulation of autophagic bodies in vacuoles was examined using an optical microscope. Typical accumulation of autophagic bodies was observed in wild-type cells and $\Delta atg16$ cells expressing wild-type or D25A Atg16 (Fig. 5B, a,c,f), whereas no such accumulation was observed in either $\Delta atg16$ cells or those expressing the R35A or F46A mutants of Atg16 (Fig. 5B, b,d,e). These results support the notion that direct interaction between Atg5 and Atg16 is crucial for autophagy.

The Atg12-Atg5-Atg16 complex localizes to the PAS and plays a crucial role in autophagosome formation (12), where Atg5 and Atg16 but not Atg12 is necessary for the localization. Thus we next studied whether Atg16 mutants can localize to the PAS using YFP-tagged Atg16 in $\Delta atg16$ yeast strains. Wild-type Atg16 localized to a punctate structure proximal to the vacuole, which corresponds to the PAS (Fig. 5C, top). The Atg16 D25A mutant also localized to a similar

dot structure (Fig. 5C, bottom). In contrast, Atg16 R35A and F46A mutants did not localize to any punctate structures and spread in the cytosol (Fig. 5C, middle two panels). These results suggest that the direct interaction between Atg5 and Atg16 is essential for the localization of Atg16 to the PAS.

The expression of Atg8 is significantly enhanced under starvation conditions and the Atg8-PE level dramatically increases compared with that of unconjugated Atg8. Atg8-PE formation was severely diminished in the absence of the Atg12-Atg5 conjugate (12). Moreover, in the absence of Atg16, Atg8-PE formation was reduced and unconjugated Atg8 was accumulated under starvation conditions but not under nutrient-rich conditions (12). Therefore, we examined Atg8-PE formation in $\Delta atg16$ cells expressing Atg16 mutants. In cells expressing the Atg16 D25A mutant, Atg8-PE formation was observed to a similar extent to those expressing wild-type Atg16 even under starvation conditions (Fig. 5D). In contrast, unconjugated Atg8 but not Atg8-PE was accumulated in cells expressing the R35A or F46A mutants of Atg16 under starvation conditions to a similar extent to cells transformed with a control vector (Fig. 5D). These results suggest that the direct interaction between Atg5 and Atg16 is critical for efficient Atg8-PE formation under starvation conditions.

DISCUSSION

In the yeast *Saccharomyces cerevisiae*, many Atg proteins have been observed to cluster into a punctuate structure proximal to the vacuole, called the PAS. From the PAS, isolation membranes, the precursors of autophagosomes, are thought to be formed. The Atg12-Atg5-Atg16 complex was found to be localized to the PAS, suggesting that the complex plays a critical role in autophagosome formation. Thus far, it has been reported that the localization of the Atg12-Atg5-Atg16 complex to the PAS depends on both Atg5 and Atg16, but not Atg12 (12). However, the significance of the direct complex formation between Atg5 and Atg16 remained unclear. We have shown herein that the direct interaction between Atg5 and Atg16 is crucial not only for the localization, but also for autophagy (Fig. 5). Furthermore, we have also shown that the binding site for Atg16 and the conjugation site for Atg12 are located on the opposite sides of Atg5 (Fig. 1). These results

suggest that the Atg12-Atg5-Atg16 complex localizes to the PAS using the surface formed by both Atg5 and Atg16. The autophagy-specific phosphatidylinositol 3-kinase (PI3-kinase) complex, which itself localizes to the PAS (30), is known to be essential for targeting the Atg12-Atg5 conjugate to the PAS (12). Since PI3-kinase produces phosphoinositide 3-phosphate (PI3-P), it can be speculated that PI3-P is produced on the PAS by PI3-kinase, and then interacts with the Atg5-Atg16 complex, either directly or *via* some PI3-P binding protein(s), by which the complex is recruited to the PAS. Since the overall architecture of Atg5-Atg16(1-57) is quite novel and the structure contains no known binding motifs for PI3-P, the interaction between the Atg5-Atg16 complex and PI3-P, if it exists, is also thought to be novel.

Atg3, Atg7, Atg8 (processed form), and ATP are necessary and sufficient for Atg8-PE formation *in vitro* (19). However, in addition to these factors, the Atg12-Atg5 conjugate is also required for Atg8-PE formation *in vivo* (12), and the significance of Atg12 in Atg8-PE formation was shown by mutational analyses (31). The expression level of Atg8 is dramatically enhanced upon nutrient depletion. Under such conditions, Atg16 is also required for the efficient formation of Atg8-PE (12). We demonstrated here that Atg16 mutants that lack affinity to Atg5 do not promote Atg8-PE formation (Fig. 5D). Since most Atg5 exists as a conjugate with Atg12 *in vivo*, this result suggests that Atg16 promotes Atg8-PE formation as a complex with the Atg12-Atg5 conjugate. This activity of the Atg12-Atg5-Atg16 complex is similar to that of E3 enzymes in the ubiquitin system. In most cases, E3 binds to both E2 and a target protein, thus mediating the transfer of ubiquitin between them. The Atg5-Atg16(1-57) complex shows no structural similarity to E3 enzymes, and the molecular mechanism by which the Atg12-Atg5-Atg16 complex promotes Atg8-PE formation is still unclear. Since complex formation between Atg16 and the Atg12-Atg5 conjugate is crucial for both the promotion of Atg8-PE formation and targeting of the Atg12-Atg5-Atg16 complex to the PAS, these two events appear to have a strong relationship. Atg12 was shown to interact with Atg3, the E2 enzyme for Atg8 lipidation, by yeast two-hybrid screening (32). Taken together, these results suggest that the Atg12-Atg5-Atg16 complex binds to both Atg3 and the PAS, thus

promoting the transfer of Atg8 between Atg3 and PE at the PAS. This idea is consistent with the observation that the Atg12-Atg5-Atg16 complex is also crucial for the localization of

Atg8-PE to the PAS. However, further studies are required to elucidate this mechanism, including the identity of the PAS itself.

REFERENCES

1. Seglen, P. O., and Bohley, P. (1992) *Experientia* **48**, 158-172
2. Takeshige, K., Baba, M., Tsuboi, S., Noda, T., and Ohsumi, Y. (1992) *J. Cell Biol.* **119**, 301-311
3. Hara, T., Nakamura, K., Matsui, M., Yamamoto, A., Nakahara, Y., Suzuki-Migishima, R., Yokoyama, M., Mishima, K., Saito, I., Okano, H., and Mizushima, N. (2006) *Nature* **441**, 885-889
4. Komatsu, M., Waguri, S., Chiba, T., Murata, S., Iwata, J., Tanida, I., Ueno, T., Koike, M., Uchiyama, Y., Kominami, E., and Tanaka, K. (2006) *Nature* **441**, 880-884
5. Ogawa, M., Yoshimori, T., Suzuki, T., Sagara, H., Mizushima, N., and Sasakawa, C. (2005) *Science* **307**, 727-731
6. Nakagawa, I., Amano, A., Mizushima, N., Yamamoto, A., Yamaguchi, H., Kamimoto, T., Nara, A., Funao, J., Nakata, M., Tsuda, K., Hamada, S., and Yoshimori, T. (2004) *Science* **306**, 1037-1040
7. Kuma, A., Hatano, M., Matsui, M., Yamamoto, A., Nakaya, H., Yoshimori, T., Ohsumi, Y., Tokuhisa, T., and Mizushima, N. (2004) *Nature* **432**, 1032-1036
8. Tsukada, M., and Ohsumi, Y. (1993) *FEBS Lett.* **333**, 169-174
9. Mizushima, N., Noda, T., Yoshimori, T., Tanaka, Y., Ishii, T., George, M. D., Klionsky, D. J., Ohsumi, M., and Ohsumi, Y. (1998) *Nature* **395**, 395-398
10. Shintani, T., Mizushima, N., Ogawa, Y., Matsuura, A., Noda, T., and Ohsumi, Y. (1999) *EMBO J.* **18**, 5234-5241
11. Kuma, A., Mizushima, N., Ishihara, N., and Ohsumi, Y. (2002) *J. Biol. Chem.* **277**, 18619-18625
12. Suzuki, K., Kirisako, T., Kamada, Y., Mizushima, N., Noda, T., and Ohsumi, Y. (2001) *EMBO J.* **20**, 5971-5981
13. Mizushima, N., Yamamoto, A., Hatano, M., Kobayashi, Y., Kabeya, Y., Suzuki, K., Tokuhisa, T., Ohsumi, Y., and Yoshimori, T. (2001) *J. Cell Biol.* **152**, 657-668
14. Mizushima, N., Noda, T., and Ohsumi, Y. (1999) *EMBO J.* **18**, 3888-3896
15. Kim, J., Huang, W. P., and Klionsky, D. J. (2001) *J. Cell Biol.* **152**, 51-64
16. Mizushima, N., Kuma, A., Kobayashi, Y., Yamamoto, A., Matsubae, M., Takao, T., Natsume, T., Ohsumi, Y., and Yoshimori, T. (2003) *J. Cell Sci.* **116**, 1679-1688
17. Kirisako, T., Ichimura, Y., Okada, H., Kabeya, Y., Mizushima, N., Yoshimori, T., Ohsumi, M., Takao, T., Noda, T., and Ohsumi, Y. (2000) *J. Cell Biol.* **151**, 263-276
18. Ichimura, Y., Kirisako, T., Takao, T., Satomi, Y., Shimonishi, Y., Ishihara, N., Mizushima, N., Tanida, I., Kominami, E., Ohsumi, M., Noda, T., and Ohsumi, Y. (2000) *Nature* **408**, 488-492
19. Ichimura, Y., Imamura, Y., Emoto, K., Umeda, M., Noda, T., and Ohsumi, Y. (2004) *J. Biol. Chem.* **279**, 40584-40592
20. Suzuki, N. N., Yoshimoto, K., Fujioka, Y., Ohsumi, Y., and Inagaki, F. (2005) *Autophagy* **1**, 119-126
21. Matsushita, M., Suzuki, N. N., Fujioka, Y., Ohsumi, Y., and Inagaki, F. (2006) *Acta Crystallograph. Sect. F Struct. Biol. Cryst. Commun.* **62**, 1021-1023
22. Otwinowski, Z., and Minor, W. (1997) *Methods Enzymol.* **276**, 307-326
23. Brünger, A. T., Adams, P. D., Clore, G. M., DeLano, W. L., Gros, P., Grosse-Kunstleve, R. W., Jiang, J. S., Kuszewski, J., Nilges, M., Pannu, N. S., Read, R. J., Rice, L. M., Simonson, T., and Warren, G. L. (1998) *Acta Crystallogr. D. Biol. Crystallogr.* **54**, 905-921
24. Jones, T. A., Zou, J. Y., Cowan, S. W., and Kjeldgaard, M. (1991) *Acta Crystallogr. A.* **47 (Pt 2)**, 110-119
25. Emsley, P., and Cowtan, K. (2004) *Acta Crystallogr. D. Biol. Crystallogr.* **60**, 2126-2132
26. Robinson, J. S., Klionsky, D. J., Banta, L. M., and Emr, S. D. (1988) *Mol. Cell. Biol.* **8**,

- 4936-4948
27. Stroupe, M. E., Leech, H. K., Daniels, D. S., Warren, M. J., and Getzoff, E. D. (2003) *Nat. Struct. Biol.* **10**, 1064-1073
 28. Swanson, K. A., Kang, R. S., Stamenova, S. D., Hicke, L., and Radhakrishnan, I. (2003) *EMBO J.* **22**, 4597-4606
 29. Sugawara, K., Suzuki, N. N., Fujioka, Y., Mizushima, N., Ohsumi, Y., and Inagaki, F. (2004) *Genes Cells* **9**, 611-618
 30. Obara, K., Sekito, T., and Ohsumi, Y. (2006) *Mol. Biol. Cell* **17**, 1527-1539
 31. Hanada, T., and Ohsumi, Y. (2005) *Autophagy* **1**, 110-118
 32. Uetz, P., Giot, L., Cagney, G., Mansfield, T. A., Judson, R. S., Knight, J. R., Lockshon, D., Narayan, V., Srinivasan, M., Pochart, P., Qureshi-Emili, A., Li, Y., Godwin, B., Conover, D., Kalbfleisch, T., Vijayadamar, G., Yang, M., Johnston, M., Fields, S., and Rothberg, J. M. (2000) *Nature* **403**, 623-627

FOOTNOTES

* We thank Dr. D. J. Klionsky for providing the anti-API antibody, and R. Ichikawa for technical support. The synchrotron radiation experiments were performed at the BL41XU in the SPring-8 with the approval of the Japan Synchrotron Radiation Research Institute (JASRI) (Proposal No. 2004B0839). This work was supported by Grant-in-Aids for Young Scientists (B) 17790048 and for priority areas, and the National Project on Protein Structural and Functional Analyses from the Ministry of Education, Culture, Sports, Science, and Technology, Japan. This work was carried out under the NIBB Cooperative Research Program (4-148).

¹The abbreviations used are: PE, phosphatidylethanolamine; LC3, microtubule-associated protein light chain 3; GST, glutathione *S*-transferase; SeMet, selenomethionine; MAD, multi-wavelength anomalous diffraction; MIR, multiple isomorphous replacement; Cvt, cytoplasm-to-vacuole targeting; API, aminopeptidase I; Ubl, ubiquitin-like.

FIGURE LEGENDS

Fig. 1. Structure of the Atg5·Atg16(1-57) complex. *A*, Ribbon diagram of the Atg5·Atg16(1-57) complex. α -Helices are labeled (α 1- α 9) and indicated by red helical ribbons, and β -strands are labeled (β 1- β 10) and indicated by cyan arrows. The N and C termini of Atg5 are denoted by N₅ and C₅, respectively, while those of Atg16 are denoted by N₁₆ and C₁₆, respectively. Residues adjacent to the disordered regions are numbered. This figure and figures 3 and 4A were prepared using PyMOL (<http://pymol.sourceforge.net>). *B*, Topology of Atg5. α -Helices are indicated by rectangles and β -strands by arrows. Secondary structure elements of UblA, UblB, and HR are colored yellow, red, and green, respectively, while α 1 is colored orange. Loop regions are indicated by black lines except for L1 and L2, which are indicated by gray lines. Residues at the termini of secondary structure elements are numbered. The location of Lys-149 is indicated by a black circle. *C*, Stereoview of the ribbon diagram of Atg5. UblA, UblB, HR, α 1, L1, and L2 are colored as in *B*. The side-chain of Lys-149 is indicated by a blue stick model. The N and C termini are denoted by N and C, respectively.

Fig. 2. Sequence alignment of Atg5 homologs. The secondary structure elements (colored as in Fig. 1*B*) and residue numbers of ScAtg5 are shown above the alignment. Conserved hydrophobic residues are colored light gray, whereas conserved non-hydrophobic residues are colored dark gray. Sequences of LC3 and ubiquitin are also aligned with UblA and UblB of Atg5 based on their three-dimensional structures.

Fig. 3. Intramolecular interactions constituting the architecture of Atg5. *A*, Ribbon diagrams of the interaction between UblA and UblB (left) and that between UIM and ubiquitin (right). UblA and UIM are colored yellow, whereas UblB and ubiquitin are colored red. The side-chains of Ile-44 and His-68

of ubiquitin and their equivalent residues, Ile-251 and Thr-280, of UblB are shown as stick models. *B*, Ribbon diagrams of the interaction between HR and UblB (left) and that between the N-terminal and ubiquitin-core regions of LC3 (right). The HR and N-terminal regions of LC3 are colored green, UblB and the ubiquitin-core of LC3 are colored red, and UblA is colored yellow. The side-chains of the residues involved in these interactions as well as Lys-149 are shown as stick models. Residues observed in both Atg5 and LC3 are labeled with blue letters. *C*, A ribbon diagram of the interaction between L1 and UblA. UblA, HR, and L1 are colored yellow, green, and gray, respectively. Four conserved hydrophobic residues of L1 and two conserved tryptophan of UblA are shown as stick models. *D*, A ribbon diagram of the interaction of $\alpha 1$ with its neighbors. $\alpha 1$, UblA, UblB, HR, and Atg16 are colored orange, yellow, red, green, and cyan, respectively. The side-chains of the residues involved in the interaction between $\alpha 1$ and its neighbors are shown as stick models.

Fig. 4. Structural basis of the interaction between Atg5 and Atg16. *A*, An entire view of the interaction between Atg5 and Atg16. Atg5 is shown with the surface representation colored as in Fig. 1B, and Atg16 is shown as a cyan ribbon diagram. The side-chains of Atg16 are shown as stick models in which oxygen, nitrogen, and sulfur atoms are colored red, blue, and yellow, respectively. *B*, Stereoview of the detailed interaction between Atg5 and Atg16. Atg5 is colored as in Fig. 1B, whereas Atg16 is colored cyan. Residues involved in the interaction between Atg5 and Atg16 are shown as stick models, in which oxygen, nitrogen, and sulfur atoms are colored red, blue, and yellow, respectively. Residues forming hydrophilic interactions are connected with broken lines. *C*, *In vitro* pull-down assay between Atg5 and Atg16 mutants. GST-fused Atg16 and its mutants were incubated with hexa-histidine-tagged Atg5. Proteins pulled down with glutathione-Sepharose 4B resin were subjected to SDS-PAGE and stained with Coomassie Brilliant Blue.

Fig. 5. Interaction between Atg5 and Atg16 is essential for autophagy. *A*, API maturation in cells expressing Atg16 mutants were monitored. Cells (SEY6210 background) grown in SD + CA + AdeUra medium were collected during the logarithmic phase (starvation -) and at 4 h after transfer into SD (-N) medium (starvation +). The prepared lysates were separated by SDS-PAGE and subjected to immunoblotting with anti-API antibody. *B*, The accumulation of autophagic bodies was examined on the BJ2168 background, which lacks vacuolar proteases. Cells in the logarithmic phase of growth were transferred to S (-NC) medium. After culture for 4 h in S (-NC) medium, cells were observed by phase-contrast microscopy. WT cells bearing an empty vector (a) and $\Delta atg16$ cells bearing an empty vector (b) or expressing Atg16 (c), Atg16 R35A (d), Atg16 F46A (e), or Atg16 D25A (f) are shown. Autophagic bodies were indicated by arrowheads. Bar, 5 μ m. *C*, Intracellular localization of Atg16 mutants was observed. Cells (SEY6210 background) expressing YFP-tagged Atg16 mutants were grown in SD + CA + AdeUra medium to logarithmic phase and transferred to SD (-N) medium. After culture for 4 h in SD (-N) medium, cells were subjected to fluorescence microscopy. Arrows indicate Atg16 mutants accumulated at the PAS. Bar, 5 μ m. *D*, Atg8 lipidation in cells expressing Atg16 mutants was monitored. Cells (SEY6210 background) grown in SD + CA + AdeUra medium were collected during the logarithmic phase (starvation -) and at 4 h after transfer into SD (-N) medium (starvation +). The prepared lysates were separated by SDS-PAGE and subjected to immunoblotting with anti-Atg8 antibody.

Table I. Data collection and phasing statistics

Data set	MIR phasing			MAD phasing		
	Native2	K ₂ (HgI ₄)	(NH ₄) ₂ PtCl ₂		Se-Met	
Data collection statistics						
X-ray source	Cu K α	Cu K α	Cu K α	BL41XU	BL41XU	BL41XU
Wavelength (Å)	1.5418	1.5418	1.5418	0.9792	0.9795	0.9750
Soaking conditions		1 mM, 30 min	10 mM, 5 min			
Resolution range (Å)	50.00-2.50	50.00-3.30	50.00-3.60	50.00-2.00	50.00-2.00	50.00-2.00
Outer shell (Å)	2.59-2.50	3.42-3.30	3.73-3.60	2.07-2.00	2.07-2.00	2.07-2.00
Cell parameters						
<i>a</i> (Å)	66.23	66.22	66.11	66.28	66.27	66.28
<i>b</i> (Å)	104.34	104.65	104.84	104.85	104.85	104.86
<i>c</i> (Å)	112.23	112.03	111.69	112.91	112.91	112.91
β (°)	92.13	92.01	92.00	92.35	92.35	92.35
Observed reflections	99,889	78,723	50,333	274,319	273,628	271,429
Unique reflections	51,153	22,841	15,864	147,491	147,086	145,906
Completeness (%)	96.5(95.1)	98.5(96.5)	87.0(72.0)	71.6(19.1)	71.2(17.6)	70.8(13.5)
$R_{\text{merge}}(I)^a$	0.058(0.352)	0.098(0.286)	0.111(0.284)	0.052(0.252)	0.051(0.242)	0.051(0.242)
$I/\sigma(I)$	9.8(1.74)	5.6(2.46)	7.0(3.5)	9.8(1.81)	9.8(1.88)	9.9(1.91)
Phasing statistics						
Resolution range (Å)	50.00-3.50	50.00-3.50	50.00-3.50	50.00-3.00	50.00-3.00	50.00-3.00
No. of sites		8	2	35	35	35
Phasing power		1.02	0.76	1.47/0.56 ^b	1.47/0.90 ^b	0.75/0 ^b
Mean figure of merit	0.5202					

^a $R_{\text{merge}}(I) = (\sum \sum |I_i - \langle I \rangle|) / \sum \sum I_i$, where I_i is the intensity of the i th observation and $\langle I \rangle$ is the mean intensity. Values in parentheses refer to the outer shell.

^b Values to the left and the right of a slash refer to the phasing power for anomalous and dispersive, respectively.

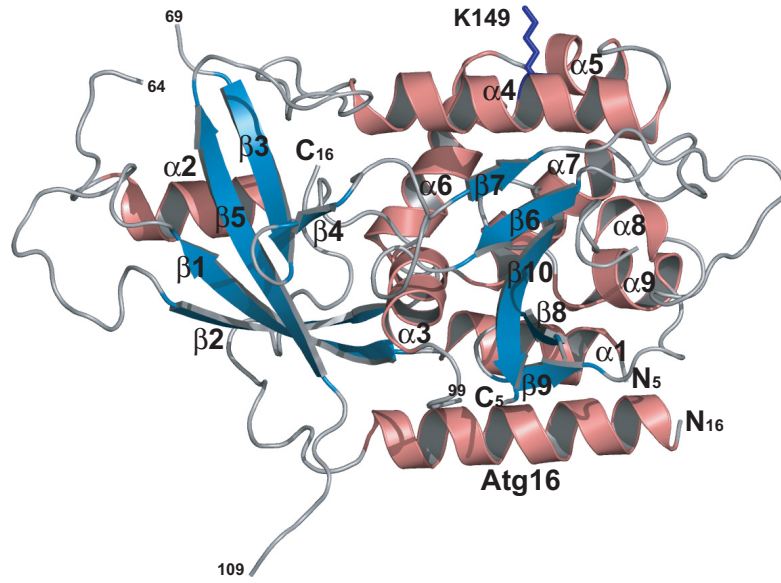
Values in parentheses refer to the outer shell.

Table II. Refinement statistics

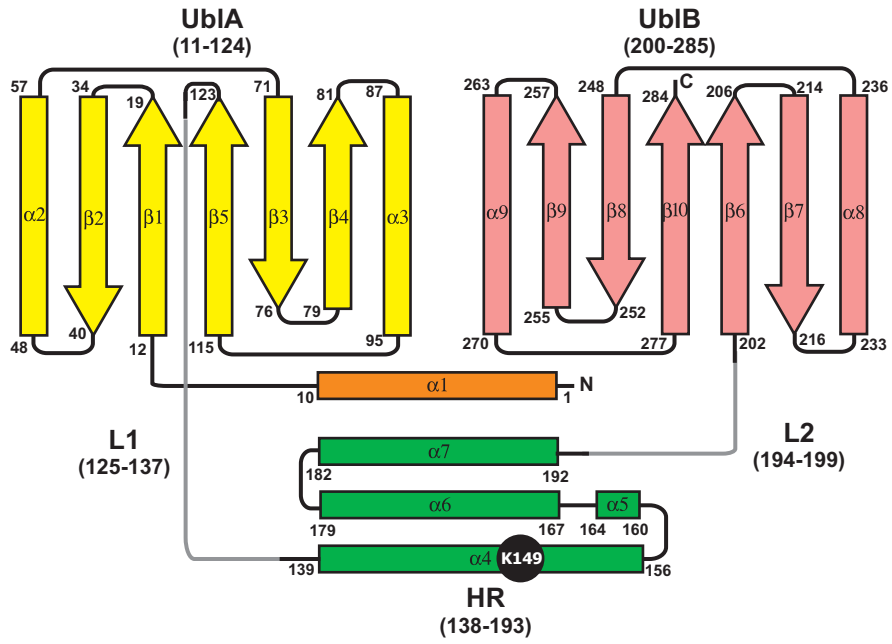
		Atg5·Atg16(1-46)	Atg5·Atg16(1-57)
Resolution range (Å)		50.00-2.20	50.00-1.97
Reflections used		74,879	28,960
No. of protein atoms		8,882	2,429
No. of water molecules		321	244
R/R_{free}		0.222/0.250	0.215/0.245
Rmsd from ideality	Length (Å)	0.006	0.005
	Angles (°)	1.3	1.2

Figure 1

A



B



C

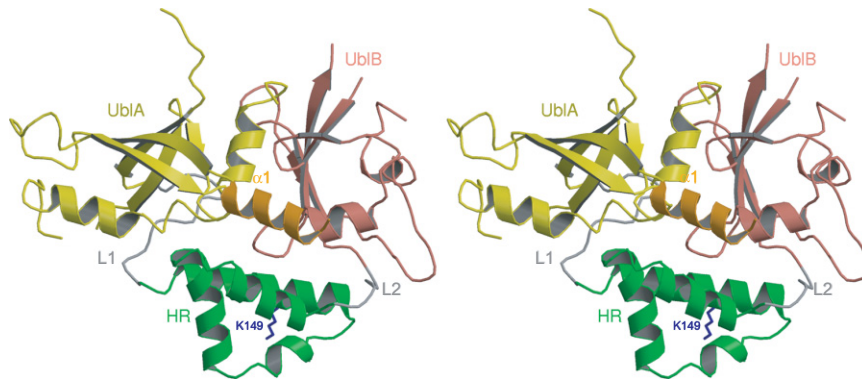


Figure 2

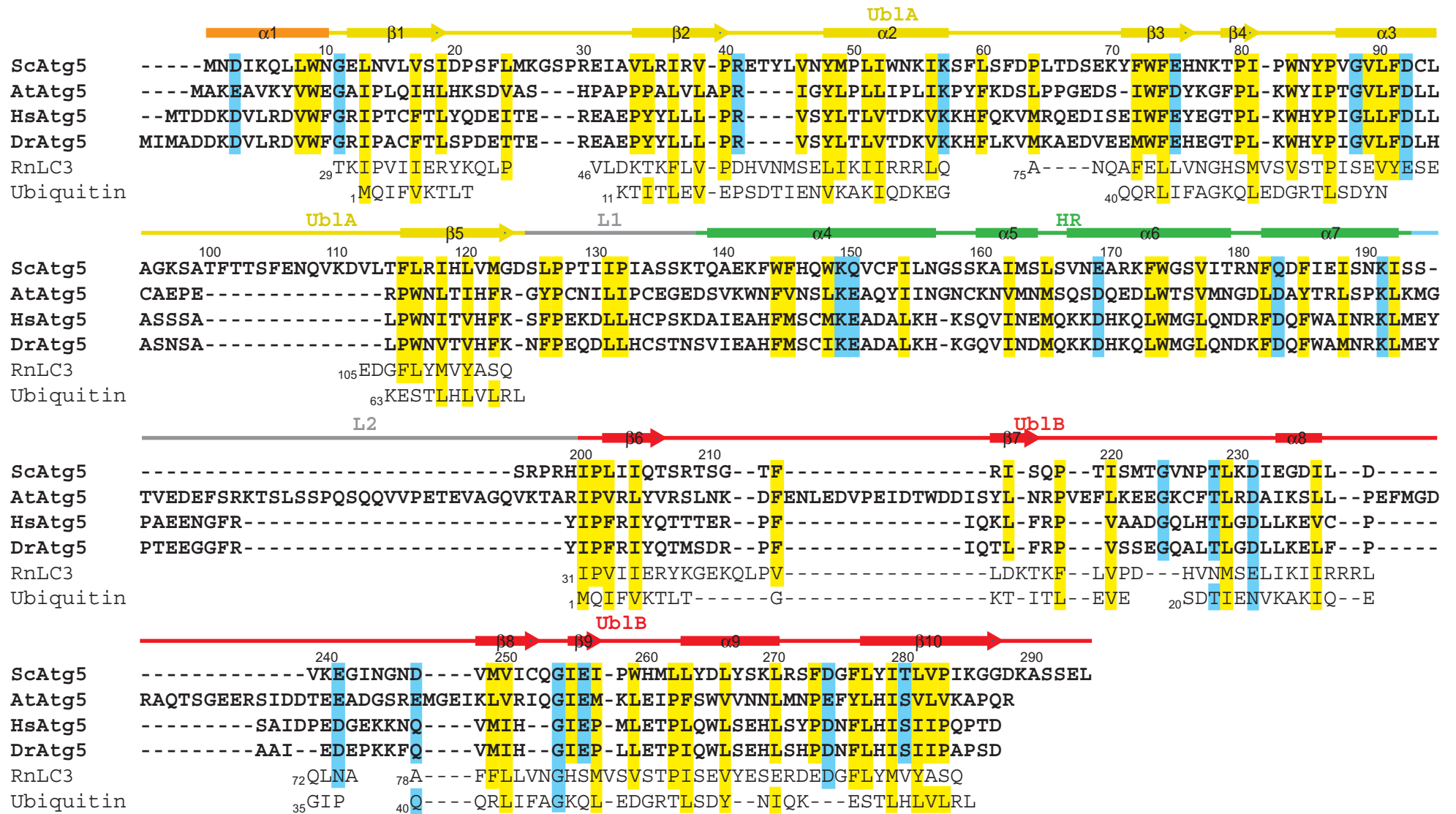
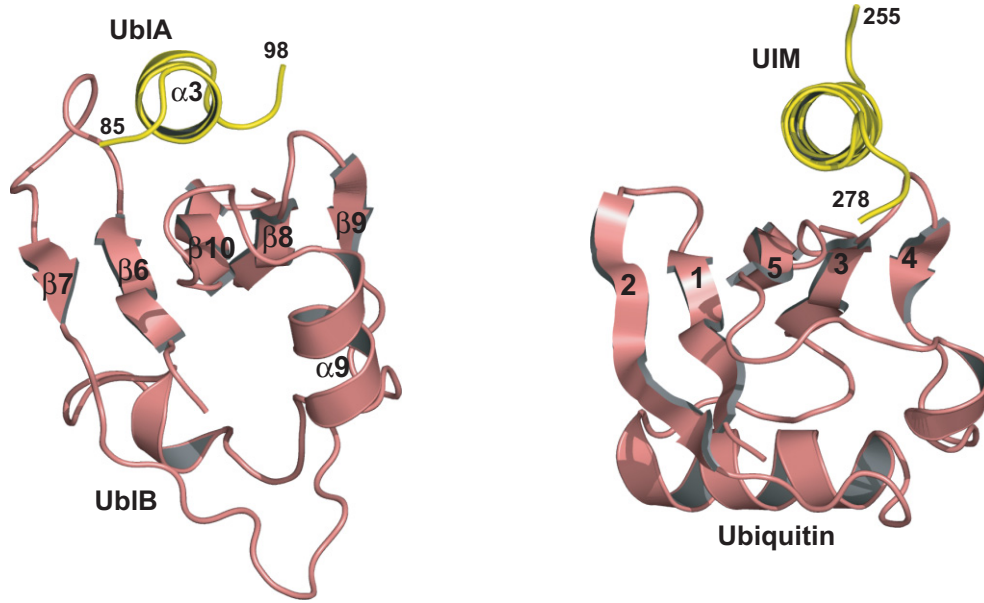
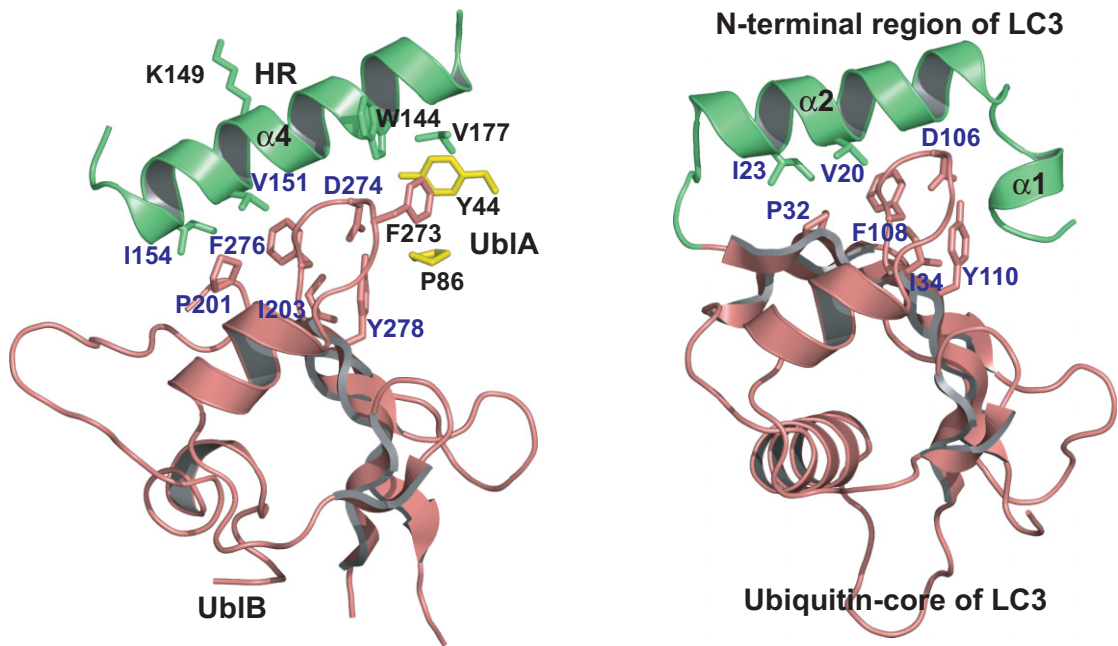


Figure 3

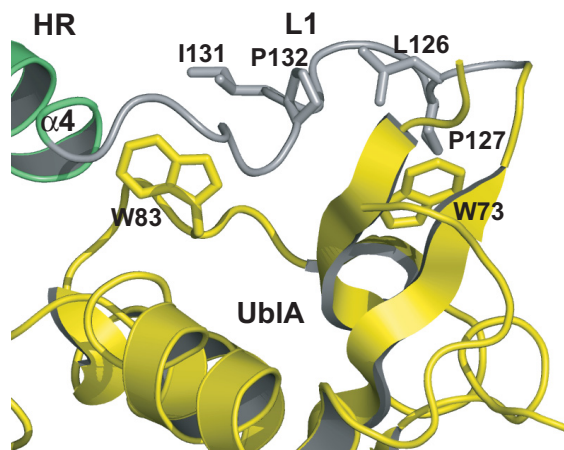
A



B



C



D

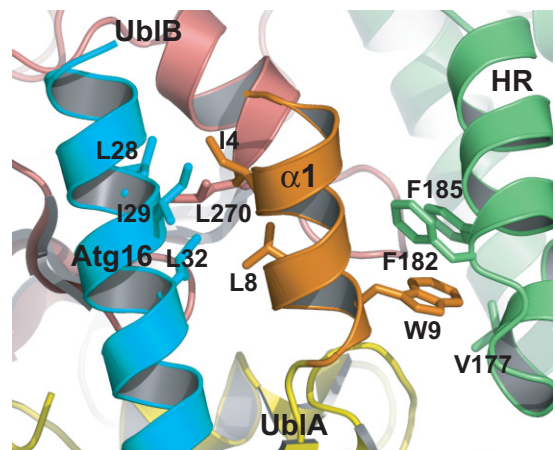


Figure 5

